Dielectronic and Trielectronic Recombination Rate Coefficients of Be-Like Ar^{14+}

Z. K. Huang[1], W. Q. Wen[1], X. Xu[2], S. Mahmood[1], S. X. Wang[2], H. B. Wang[1], L. J. Dou[1], N. Khan[1, 3], N. R. Badnell[6], S. P. Preval[6], S. Schippers[7], T. H. Xu[4], Y. Yang[4], K. Yao[4], W.Q. Xu[5], X. Y. Chuai[1], X. L. Zhu[1], D. M. Zhao[1], L. J. Mao[1], X. M. Ma[1], J. Li[1], R. S. Mao[1], Y. J. Yuan[1], B. Wu[1], L. N. Sheng[1], J. C. Yang[1], H. S. Xu[1], L. F. Zhu[2] and X. Ma[1]

[1] Institute of Modern Physics, Chinese Academy of Sciences, 730000, Lanzhou, China;
wenweiqiang@impcas.ac.cn, x.ma@impcas.ac.cn

[2] Hefei National Laboratory for Physical Sciences at Microscale, Department of Modern Physics, University of Science and Technology of China, 230026, Hefei, China

[3] University of Chinese Academy of Sciences, 100049, Beijing, China

[4] Institute of Modern Physics, Fudan University, 200433, Shanghai, China

[5] Department of Mathematics and Physics, Bengbu University, 233000, Bengbu, China

[6] Department of Physics, University of Strathclyde, Glasgow G4 0NG, UK

[7] I. Physikalisches Institut, Justus-Liebig-Universität Gießen, 35392 Giessen, Germany

ABSTRACT

Electron-ion recombination of Be-like $^{40}Ar^{14+}$ has been measured by employing the electron-ion merged-beams method at the cooler storage ring CSRm. The measured absolute recombination rate coefficients for collision energies from 0 to 60 eV are presented, covering all dielectronic recombination (DR) resonances associated with $2s^2 \rightarrow 2s2p$ core transitions. In addition, strong trielectronic recombination (TR) resonances associated with $2s^2 \rightarrow 2p^2$ core transitions were observed. Both DR and TR processes lead to series of peaks in the measured recombination spectrum, which have been identified by the Rydberg formula. Theoretical calculations of recombination rate coefficients were performed using the state-of-the-art multi-configuration Breit-Pauli (MCBP) atomic structure code AUTOSTRUCTURE to compare with the experimental results. The plasma rate coefficients for DR+TR of Ar^{14+} were deduced from the measured electron-ion recombination rate coefficients in the temperature range from 10^3 to10^7 K, and compared with calculated data from the literature. The experimentally-derived plasma rate coefficients are 60% larger and 30% lower than the previously recommended atomic data for the temperature ranges of photoionized plasmas and collisionally-ionized plasmas, respectively. However, good agreement was found between experimental results and the calculations by (Gu 2003) and (Colgan et al. 2003). The plasma rate coefficients deduced from experiment and calculated by the current AUTOSTRUCTURE code show agreement that is better than 30% from 10^4 to10^7 K. The present results constitute a set of bench-mark data for use in astrophysical modeling.

Keywords: atomic data – atomic processes - plasmas

1. INTRODUCTION

It has been estimated that more than 90% of the visible matter in the universe is in plasma state (Müller 2008). Astrophysical plasmas can be divided into two main classes, i) the collisionally ionized plasma formed in stars, supernova remnants and galaxies, and ii) photoionized plasmas formed in the sources such as planetary nebulae, X-ray binaries and active galactic nuclei. Various types of reactions take place in astrophysical plasmas, such as electron collision excitation, electron impact ionization, and electron-ion recombination (Savin 2007). Emission features originating from these plasmas are essential in deducing the properties of the plasmas, such as temperature, density and elemental abundances (Beiersdorfer 2003; Kallman & Palmeri 2007). Electron-ion recombination processes such as radiative recombination (RR) and dielectronic recombination (DR) contribute substantially to the line emission for photoionized plasmas. In addition, the ionization balance of a plasma is determined by the relative rates of ionization and recombination.

In order to understand astrophysical plasmas, space-based observatories, such as Chandra and XMM-Newton, have been launched to observe x-ray emission from various astrophysical objects (Paerels & Kahn 2003). All the observed emission and absorption lines have to be explained by plasma modelling, and most of the input atomic data for these plasma models are from theory. However, many theories cannot calculate the DR rate coefficients with sufficient precision and have large uncertainties especially at low energies due to sensitivity in the positioning of resonances. As a result, precise electron-ion recombination data from experiment are required to explain the astrophysical observations and to benchmark the theory. With these data, information pertaining to these astrophysical objects, such as the structure, elemental composition, energy balance, and temperature distribution, can be investigated (Kallman & Palmeri 2007).

The importance of DR in a plasma was recognized for the first time by Burgess in 1964 (Burgess 1964). Since then, DR is considered as an important process in atomic physics and plasma physics. DR experiments on highly charged ions employing the electron-ion merged beams technique have been developed for more than two decades at heavy ion storage rings, i.e., the TSR at MPIK in Heidelberg (Schippers 2015), the ESR at GSI in Darmstadt (Brandau & Kozhuharov 2012), Germany, and the CRYRING at MSL in Stockholm, Sweden (Schuch & Böhm 2007). **The main cooler storage ring (CSRm)** equipped with an electron cooler provides an ideal research platform for electron-ion recombination experiments of highly charged ions at heavy ion research facility in Lanzhou (Huang et al. 2017). More details about DR experiments at storage rings can be found in the recent reviews of (Brandau & Kozhuharov 2012; Brandau et al. 2015; Müller 2008; Schippers 2015) and in the references cited therein. Recent reviews of experimental DR measurements for astrophysics application have been given by (Schippers 2012).

Argon is one of the most abundant heavy elements in the universe and also in the solar system. The emission lines from argon have already been observed and were used for plasma diagnostics (Dere et al. 2001). In addition, Be-like argon has been observed in hot solar plasmas where the temperature is ~10^6 K (Bhatia & Landi 2008). The intensity ratios of the emission lines from Ar^{14+} were used to diagnose coronal plasmas (Landi et al. 2001; Saloman 2010). Therefore, investigating the recombination of Be-like Ar will provide very useful information for astrophysics. It is noted that the emission lines from highly charged argon have been investigated at an electron beam ion trap EBIT (Lepson et al. 2003; Träbert et al. 2000). Here, we present absolute rate coefficients for electron-ion recombination of Be-like argon from an experiment at the main cooler storage ring CSRm and from theoretical calcuations using the AUTOSTRUCTURE code.

For Be-like Ar^{14+}, the experimental electron-ion collision energy range was 0-60 eV. The most significant recombination channels in this energy range are

$$\mathrm{Ar}^{14+}(2s^2\ {}^1S_0)+e^- \rightarrow \left\{\begin{array}{l} \mathrm{Ar}^{13+}[2s^2nl],\ \ \mathrm{RR}; \\ \mathrm{Ar}^{13+}[2s2p({}^3P_{0,1,2})nl],\ \ n\geq 10,\ \ \mathrm{DR}; \\ \mathrm{Ar}^{13+}[2s2p({}^1P_1)nl],\ \ n\geq 7,\ \ \mathrm{DR}; \\ \mathrm{Ar}^{13+}[2p^2({}^3P_{0,1,2};{}^1D_2;{}^1S_0)nl],\ \ n\geq 6,\ \ \mathrm{TR}; \end{array}\right\} \quad (1)$$

where RR, DR, and TR denote radiative, dielectronic, and trielectronic recombination, respectively. In RR, a free electron is captured into a bound state of the ion and a photon is emitted. DR is a two-step process, a doubly excited intermediate state is formed through a resonant process involving capture of a free electron and simultaneous excitation of a bound electron, then the doubly excited state decays via photon emission such that the charge state of the recombined ion is stablized. In the case of TR, the capture is associated with the excitation of two core electrons to higher levels, and completed when the triply excited intermediate level decays by photon emmision. The excitation energies of the core electrons and lifetimes associated with ΔN= 0 (Here N is the principal quantum number of the transition core electron) DR and TR are listed in Table 1.

Table 1. Excitation energies and lifetimes for ΔN=0 of Be-like Ar^{14+} levels. Numbers in brackets denote powers of 10. The data cited from NIST is from the reference (Kramida et al. 2015).

Level	Energy		Lifetime
	NIST	(Wang et al. 2015)	
	(eV)	(eV)	(s)
$1s^2\ 2s^2\ ^1S_0$	0.00000	0.00000	∞
$1s^2\ 2s\ 2p\ ^3P_0$	28.3530	28.3604	4.2[6][a]
$1s^2\ 2s\ 2p\ ^3P_1$	29.2429	29.2509	3.436[-07]
$1s^2\ 2s\ 2p\ ^3P_2$	31.3283	31.3383	1.543[-02]
$1s^2\ 2s\ 2p\ ^1P_1$	56.0630	56.0704	1.070[-10]
$1s^2\ 2p^2\ ^3P_0$	75.0000	75.0125	1.432[-10]
$1s^2\ 2p^2\ ^3P_1$	76.2776	76.2740	1.369[-10]
$1s^2\ 2p^2\ ^3P_2$	77.9000	77.9070	1.345[-10]
$1s^2\ 2p^2\ ^1D_2$		85.4889	4.789[-10]
$1s^2\ 2p^2\ ^1S_0$	104.224	104.196	6.9199[-11]

[a]lifetime associated with E1M1 two photon transition taken from (Fritzsche, Surzhykov, & Volotka 2015)

Storage-ring electron-ion recombination experiments have been performed on a number of Be-like ions emphazising different physical topics. Astrophysical data needs were specifically addressed with DR studies of C^{2+}, N^{3+}, O^{4+} (Fogle et al. 2005), F^{5+} (Ali et al. 2013), Ne^{6+} (Orban et al. 2008), Mg^{8+}, (Schippers et al. 2004), Si^{10+} (Bernhardt et al. 2016; Orban et al. 2010), and Fe^{22+} (Savin et al. 2006). Other topics were trielectronic recombination of Cl^{13+} (Schnell et al. 2003) and hyperfine-induced transition rate measurements with Ti^{18+} (Schippers et al. 2007) and S^{12+} (Schippers et al. 2012). In addition, the Be-like ions Ge^{28+} (Orlov et al. 2009) and Xe^{50+} (Bernhardt et al. 2015) were employed to test QED and electron-electron correlation effects. It is noted that the significance of TR was first observed for Be-like Cl^{13+} (Schnell, et al. 2003) and subsequently confirmed for several ions from this isoelectronic sequence. For Be-like Mg, a distinct contribution from TR in the form of several sharp peaks was also found (Schippers, et al. 2004). Toward higher Z ions, some TR resonance features appear in the recombination spectrum of Ti^{18+} (Schippers, et al. 2007) whereas in case of Fe^{22+} only one clear peak could be attributed to TR (Savin, et al. 2006).

Here, we report the first measurement of the electron-ion recombination spectrum of Be-like Ar. The paper is structured as follows: The experimental method and the data analysis are presented in Section 2. In Section 3, we give a brief description of the theoretical method used by AUTOSTRUCTURE. In Section 4, the experimental results, including merged-beam DR rate coefficients, and also plasma rate coeffiicients, are presented and compared to currently available results in the literature. A conclusion is given in section 5.

2. EXPERIMENT AND DATA ANALYSIS

Measurements were performed at the main cooler storage ring (CSRm) at the Institute of Modern Physics (IMP) in Lanzhou, China. A detailed description of the experimental setup and method for DR experiments at the CSRm has already been given in the literature (Huang et al. 2015; Huang, et al. 2017). Here, we will only briefly describe the electron-ion recombination experiment with Be-like Ar^{14+}at the CSRm.

In the experiment $^{40}Ar^{14+}$ ions were produced from an Electron Cyclotron Resonance (ECR) ion source (Zhao et al. 2017) and accelerated to a beam energy of 6.928 MeV/u by a Sector Focused Cyclotron (SFC), and then were injected into the CSRm. The stored ion current was typically ~50 μA. The beam lifetime was about 50 seconds. The electron cooler at the CSRm was employed to cool the ion beam, and was also used as an electron target in the measurement. During the experiment, the ion beam was merged with the electron beam over an effective interaction length of L= 4.0 m in the cooler section. The electron beam was adiabatically expanded from the magnetic field of 125 mT at the electron-gun section to 39 mT at the electron-cooling section, thus a colder electron beam was generated and a higher experimental resolution could be realized. The diameter of the electron beam was measured to be ~50 mm at the cooling section, with typical electron densities being $n_e = 1.1\times10^6$ cm^{-3}.

During the measurement, the injected ion beam was first electron-cooled for several seconds in order to decrease the diameter and the momentum spread of the ion beam. Then the electron energy detuning system added a bias voltage to the cathode voltage of the electron cooler to scan the electron beam energy according to a preset timing sequence (Meng et al. 2013). This provided a nonzero relative kinetic energy between electrons and ions. Downstream of the electron cooler, the recombined ions were separated from the primary ion beam in the first bending magnet and detected by a movable scintillator particle detector with nearly 100% efficiency (Wen et al. 2013). During the measurement, a DC current transformer (DCCT) was used to monitor the ion beam current in real time. Ion and electron beam position monitors (BPM) were utilized to monitor the relative positions of the ion beam and the electron beam in the cooling section. All of the DR measurements were performed under the condition of keeping the electron beam and ion beam parallel along the axis of the cooler. In addition, a Schottky pick-up was employed to monitor the revolution frequency and the momentum spread of the ion beam, and to correct the experimental data in the off-line data analysis (Wu et al. 2013).

In the DR experiments at heavy ion storage rings, the recombination rate coefficients α can be deduced from the background subtracted recombination counting rate R at a relative energy E_{rel} between electron and ion by (Bernhardt et al. 2011):

$$\alpha(E) = \frac{R}{N_i n_e (1-\beta_e \beta_i)} \cdot \frac{C}{L} \tag{2}$$

where N_i is the number of stored ions, n_e is the density of electron beam, $\beta_e = \upsilon_e / c$ and $\beta_i = \upsilon_{ion} / c$ are the velocities of electron beam and ion beam, L is length of the effective interaction section, and C is the circumference of the storage ring.

3. THEORY

For a better understanding of the measured electron-ion recombination spectrum, a theoretical calculation using the distorted-wave collision package AUTOSTRUCTURE (Badnell 2011) was performed to calculate recombination cross-sections and rate coefficients. AUTOSTRUCTURE is a versatile code that is able to calculate energy levels, oscillator strengths, radiative/autoionization rates, and many other quantities using semi-relativistic kappa-averaged wavefunctions. The underlying theory implemented by AUTOSTRUCTURE for DR is well documented, however, we discuss it briefly here. For a target ion $X_\nu^{(Q)}$ with a residual charge Q, and initial state ν, colliding with an electron and recombining into an ion $X_f^{(Q-1)}$ with final state f, the partial DR cross section $\sigma_{f\nu}^{Q}$, energy averaged over a bin width ΔE_c, can be expressed as

$$\sigma_{f\nu}^{Q}(E_c) = \frac{(2\pi a_0 I_H)^2 \tau_0}{E_c} \sum_j \frac{\omega_j}{2\omega_\nu} \frac{\sum_l A_{j\to\nu,E_c l}^{a} A_{j\to f}^{r}}{\sum_h A_{j\to h}^{r} + \sum_{m,l} A_{j\to m,E_c l}^{a}}, \tag{3}$$

where ω_ν and ω_j are the statistical weights for the $N-$ and $(N+1)-$electron states respectively. The A^r and A^a are the radiative and autoionization rates respectively, and E_c is the energy of the continuum electron with angular momentum l, fixed by the position of the resonances. I_H is the ionization energy of the hydrogen atom, k_B is the Boltzmann constant, and $(2\pi a_0)^2 \tau_0 = 2.6741 \times 10^{-32} \mathrm{cm}^2\mathrm{s}$. The sum over l covers the angular momentum quantum numbers of the Rydberg electron. The sum over j covers all autoionization states. Lastly, the sum over h and m represents the total radiative and autoionization widths respectively.

For the N −electron core configurations, we included $2s^2$, $2s2p$, and $2p^2$, and for the (N+1)-electron, we included $2s^22p$, $2s2p^2$, and $2p^3$. No promotions from $1s^2$ are included, and are hence omitted from the configuration list. For the recombined Rydberg electron, radiative/autoionization rates were calculated explicitly for principal quantum numbers $n = 3$ up to $n = 100$, after which the rates were calculated for quasi-logarithmically spaced values of n up to $n = 1000$. Interpolation was then used to obtain the remaining n. For each n, we calculated radiative/autoionization rates for sufficiently many angular momentum quantum numbers l so as to numerically converge the total DR rate coefficient to <1% over the temperature range $Q^2(10 - 10^6)$K.

In order to compare with the experimentally-derived electron-ion recombination rate coefficients on the one hand and to calculate the plasma rate coefficient on the other hand, the calculated recombination cross section $\sigma(\upsilon)$ has to be convoluted with the appropriate electron-velocity distribution to obtain the rate coefficients,

$$\alpha(E) = \langle \upsilon\sigma \rangle = \int \upsilon\sigma(\upsilon) f(\upsilon) d^3\upsilon \quad (4)$$

where $f(\upsilon)$ is the electron-velocity distribution. In case of the merged-beams rate coefficient, it is a flattened Maxwellian (Kilgus et al. 1992) that is characterized by the longitudinal and transverse temperatures $T_\parallel$ and $T_\perp$ with respect to the propagation direction of the electron beam. In case of the plasma rate coefficient, $f(\upsilon)$ is an isotropic Maxwellian characterized by the electron temperature T_e of the plasma.

4. RESULTS AND DISCUSSION

4.1 Merged-beams DR rate coefficients

The DR spectra of Be-like $^{40}Ar^{14+}$ obtained from the DR experiment at the CSRm and from the AUTOSTRUCTURE calculations are compared and shown in Figure 1. The measured spectrum covers the whole energy range of DR resonances associated from $2s \rightarrow 2p$ (ΔN=0) core excitations. In the recombination spectrum, the resonance positions of each Rydberg state can be well approximated by the Rydberg formula:

$$E_{res} = E_{exc} - I_H \left(\frac{Q}{n} \right)^2 \quad (5)$$

where E_{exc} is the core excitation energy of the ions, which is taken from the NIST database. I_H is the ionization energy of the hydrogen atom, and Q is the charge state of the target ion. The associated Rydberg resonance series of the doubly excited intermediate levels $2s2p(^1P_1)nl$ and $2s2p(^3P_J)nl$ are indicated by vertical bars. In Figure

1 the experimental energy scale was recalibrated by a factor of 1.06 to achieve agreement with the known $2s2p(^1P_1)nl$ series limit at 56.063 eV. As shown in Figure 2, by fitting the first 13 resonance peaks at relative energy below 0.5 eV with a flattened Maxwellian function each (Kilgus, et al. 1992), the longitudinal and transversal electron temperatures were obtained, yielding $k_BT_{||}$ =2.40(6) meV and $k_BT_{\perp}$=11.91(87) meV, respectively. The peak fit results are listed in Table 2. The numbers in parentheses denote the uncertainties obtained from the fit and correspond to one standard deviation. From the fit, it is concluded that the experimental energy resolution is less than 0.07 eV full width at half maximum at relative energies around 0.2 eV.

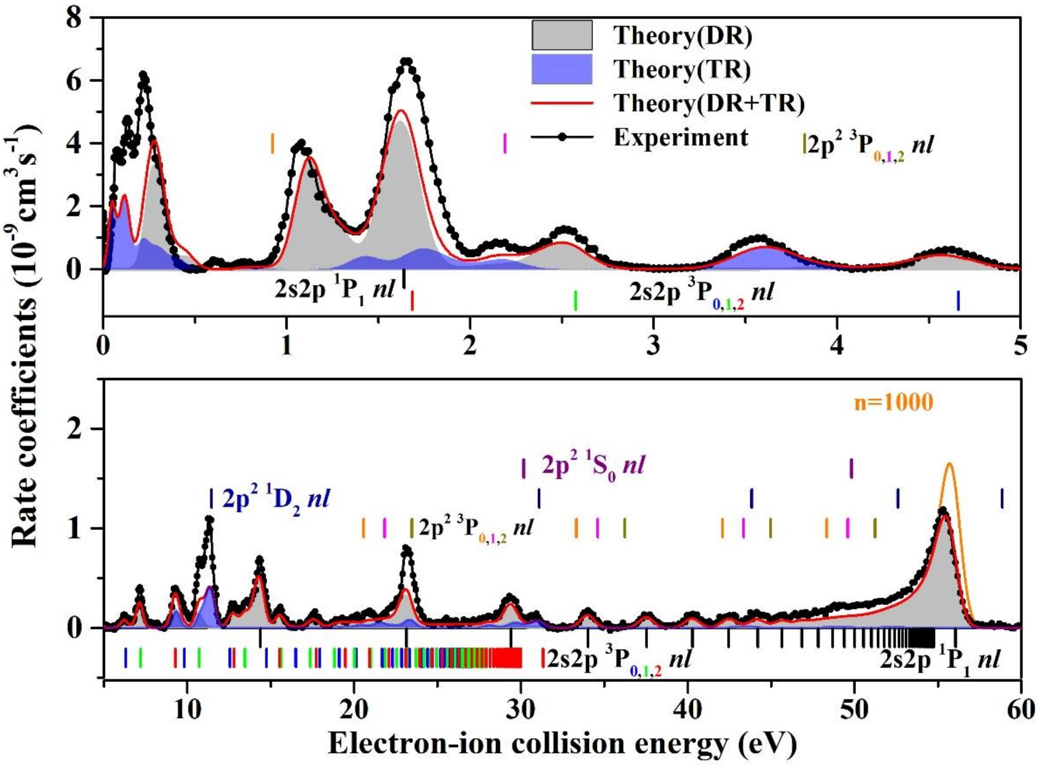

Figure 1. Electron-ion recombination rate coefficients of Be-like argon as a function of relative collision energy. The energy scale of the experimental spectrum (connected filled circles) was recalibrated by a factor of 1.06 to achieve agreement with the known $2s2p$ ($^1P_1$) nl series limit at 56.063 eV. Four $\Delta N = 0$ DR series associate with $2s^2 \rightarrow 2s2p$, $^1P_1$, $^3P_{0,1,2}$ core excitations and parts of five $\Delta N = 0$ TR series ($2s^2 \rightarrow 2p^2$, $^1S_0$, $^1D_2$, $^3P_{0,1,2}$) can be observed. The corresponding resonance positions are indicated by short bars in different colors. The calculated DR and TR rate coefficients are shown by the gray area and the blue area, respectively. The sum of the theoretical DR and TR contribution is shown as a solid red line. This curve accounts for the experimental field-ionization cutoff (see text). The orange line from 45 eV to 60 eV is the theoretical result including the full DR resonance strength up to n_{max}=1000, called the field-ionization-free recombination rate coefficient.

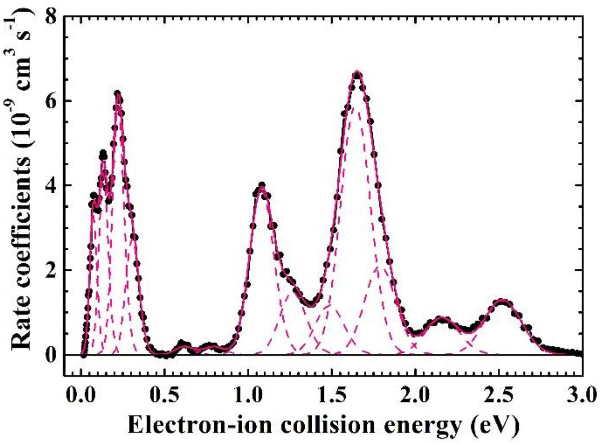

Figure 2. Peak fit (the solid pink line) to the experimental low-energy DR rate coefficient (black filled symbols). In the fit 13 δ-like resonances were convoluted with a flattened Maxwellian electron-energy distribution which is characterized by the temperatures $T_{\|}$ and $T_{\perp}$ in longitudinal and transversal direction, respectively, with respect to the electron beam propagation direction. The fit resulted in $k_B T_{\|}$ =2.40(6) meV and $k_B T_{\perp}$=11.91(87) meV. The individual peaks are shown as dashed pink lines. The fitted resonance energies and strengths are given in Table 2.

Table 2. Results of the peak fits to the experimental merged-beams DR rate coefficient at electron-ion collision energy below 3 eV (see Figure 2). The numbers in parentheses denote the uncertainties obtained from the fit and correspond to one standard deviation.

Resonance energy (eV)	Resonance strength (10^{-18} cm^2 eV)
0.08269(84)	10.57(15)
0.14436(88)	13.32(15)
0.23232(94)	17.78(17)
0.3173(14)	8.25(17)
0.629(18)	0.57(12)
0.805(21)	0.56(12)
1.091(17)	11.51(17)
1.2786(63)	0.44(16)
1.450(18)	3.46(53)
1.6524(62)	17.27(41)
1.8005(85)	6.19(65)
2.1714(74)	2.58(12)
2.5327(52)	3.81(12)

In the experiment, the recombined ions have to travel through a toroidal magnet, three quadrupole magnets and a dipole magnet before their detection. The electric field arising from these **magnetic fields can ionize** the recombined ions in high-n Rydberg levels. As a result, the ions recombining into states with the outer electron having a principal quantum number $n > n_{\rm cutoff}$ will be field-ionized in the sperating dipole magnet and cannot be detected. The critical quantum number $n_{\rm cutoff}$ for field ionization of an ion in a magnetic field can be estimated from the formula (Fogle, et al. 2005)

$$n_{cutoff} \simeq \left(6.2\times10^{8}\,V/cm\,\frac{Q^{3}}{\upsilon_i B}\right)^{1/4} \quad \textbf{(6)}$$

where Q is the charge state of the ion, υ_i is the ion velocity, and B is the magnetic field strength. In the present experiment the estimated cutoff quantum number in the charge separating dipole magnet is n_{cutoff} =74. The field-ionization effect can be seen at the series limits of $2s2p(^1P_1)nl$ around 55 eV in Figure 1. Compared with the $2s2p\ (^1P_1)nl$ series, the $2s2p(^3P_J)nl$ series limits were not observed in the DR spectra.

To fully understand the measured electron-ion recombination rate coefficients a convolution of the calculated DR resonance cross sections with the velocity distribution of the electron beam was performed by AUTOSTRUCTURE as described in Section 3. The gray area shows the theoretical DR rate coefficients with taking field ionization into account. It turns out that the resonance peaks around 0.5 eV, 4 eV and 11 eV cannot be fully identified by considering only the $2s2p(^1P_1)nl$ and $2s2p(^3P_J)nl$ DR series (Figure 1). These peaks can be attributed to TR associated $2s^2{\rightarrow}2p^2\ (^1S_0,\ ^1D_2,\ ^3P_{0,\,1,\,2})$ core double-excitations as revealed by a separate calculation of TR contributions. The calculated TR rate coefficients is shown as the blue shaded area in Figure 1. The sum of the calculated DR and TR rate coefficients is shown as a solid red line. This curve account for field ionization, i.e, it contains contribution of recombination resonance from Rydbergy levels up to 150 by taken into account of time-of-flight survival probabilities for n, as described in (Schippers et al. 2001). An additional calculation including DR and TR contributions from capture into Rydberg states up to $n_{\rm max}$=1000 from 45 eV to 60 eV is shown in Figure 1 as a solid orange line, called the field-ionization-free electron-ion recombination rate coefficient. Agreement between calculated results and experimental rate coefficients was found that better than 30% for the whole energy range. However, there is a discrepancy in resonance positions and intensity at energy less than 0.5 eV. It is due to electron-electron correlation effects. The intensity of resonances at 11 eV and 23 eV is not well produced by AUTOSTRUCTURE, either.

It should to be noted that, Be-like ions are known to have long-lived $2s2p\ ^3P_J$ levels (J=0, 1, 2) which might be present in the ion beams used for the experiment. For Be-like $^{40}Ar^{14+}$ ion which has zero nuclear spin, the lifetimes of energy levels of $2s2p(^3P_1)$ and $2s2p(^3P_2)$ are very short (as listed in Table 1) and these two metastable levels will not survive as the measurements were performed after several seconds of electron-cooling. However, the lifetime of metastable level $^3P_0$ is very long and can only decay by E1M1 two-photon transition. As a result, ions in the metastable state of $^3P_0$ are expected to have been present in the ion beam during the experiment. In order to determine the rate coefficient for the ground level of the ion, the contribution from the metastable level should be considered. However, in case of the Be-like Ar^{14+} there is an unknown fraction of metastable ions in the primary beam. As described in (Orban, et al. 2008), ion beams extracted from ECR ion sources showed a decreasing percentage of metastable content with increasing charge along the Be-like isoelectronic sequence. The metastable contents amount to 60%, 40%, 35%, 14% and 10% for C^{2+}, N^{3+}, O^{4+}, Ne^{5+} and Si^{10+} ion beams, respectively (Orban, et al. 2008; Orban, et al. 2010). Since we have also used an ECR ion source in this experiment, we estimated the maximum metastable contents amount to be 5% in the case of Be-like Ar^{14+} in our experiment. In addition, a separate calculation of electron-ion recombination for $2s2p$ $(^3P_0)$ metastable ions by AUTOSTRUCTURE was performed. In the range of the ΔN=0 DR resonances, the calculation showed very weak metastable DR resonant strengths and its contribution can be safely neglected. However, at high temperature the metastable contribution to the plasma rate coefficient becomes comparable with that from the ground because of the strong $2p$-$3d$ promotion.

The uncertainty of the experimental recombination rate coefficients is estimated to be about 30% (at a one-sigma confidence level), including 5% uncertainty of the estimated metastable content of the Ar^{14+} ions, an uncertainty of 15% due to combination of counting statistics, electron and ion beam currents, and interaction length, and an uncertainty of 20% due to the electron density distribution profile and also the position of the ion beam in this profile.

4.2 Plasma recombination rate coefficients

As mentioned above, storage ring measured electron-ion recombination rate coefficients are different from the plasma rate coefficients which were used for astrophysics modelling. In contrast to the very narrow velocity spread of the electron beam in a storage ring experiment, the electrons in astrophysical plasmas have a much broader and isotropic Maxwellian velocity spread. Therefore, the plasma rate coefficient can be obtained by convoluting the DR cross section $\sigma(E)$ with a Maxwell-Boltzmann distribution characterized by the plasma electron temperature T_e (see Eq. 4, with $E = m_e\upsilon^2/2$ and electron rest mass m_e). At electron-ion energies E >> $k_BT_\perp$ the DR cross section $\sigma(E)$ can be obtained as $\alpha(E)/\upsilon$ where $\alpha(E)$ denotes the measured merged-beams rate coeffcient. At lower energies the influence of the experimental energy spread becomes noticeable and, consequently, a different approach for the derivation of the plasma rate coefficient has to be applied. Here, this concerns about the four lowest-energy resonances from Table 2. In particular, the lowest-energy resonance appears at an energy lower than $k_BT_\perp$. For these resonances, the DR cross section as obtained from the peak fit was used in the convolution procedure following the procedure laid out by (Schippers, et al. 2004).

The experimentally-derived and theoretically calculated plasma rate coefficients as a function of electron temperature are shown in Figure 3 as the solid red line and the short-dashed red line, respectively. Both lines account for the field-ionization effect discussed above. The theoretically calculated DR and TR contributions are shown in Figure 3 by the black dashed line and the blue dot-dashed line, respectively. In order to compare the experimental result to different theoretical models, the experimental recombination rate coefficient from 45 eV to 60 eV was replaced by the AUTOSTRUCTURE calculation including recombination into states up to n_{max}=1000 (the solid orange line in Figure 1). Such a derived field-ionization-free plasma rate coefficient is shown as a gray shaded area in Figure 3. It should be noted that the contribution from recombination into resonance levels with n>1000 was considered very small and can be safely neglected.

The temperature range is from 10^3 K to 10^7 K in Figure 3. It includes the ranges of photoionized and collisionally ionized plasmas for Be-like Ar. The boundaries of these temperature ranges are displayed by vertical dashed bars. These mark the temperatures where the fractional abundance of Be-like Ar is 10% of its maximum value (Bryans, Landi, & Savin 2009; Kallman & Bautista 2001). At a temperature of 10^3 K the TR contribution is a factor of four larger than the DR contribution. In the temperature range of photoionized plasmas, the TR contribution to the total plasma rate coefficient amounts to 10%. Finally, agreement of better than 30% for the whole temperature range is found between the present experimentally-derived rate coefficients and the current AUTOSTRUCTURE calculations.

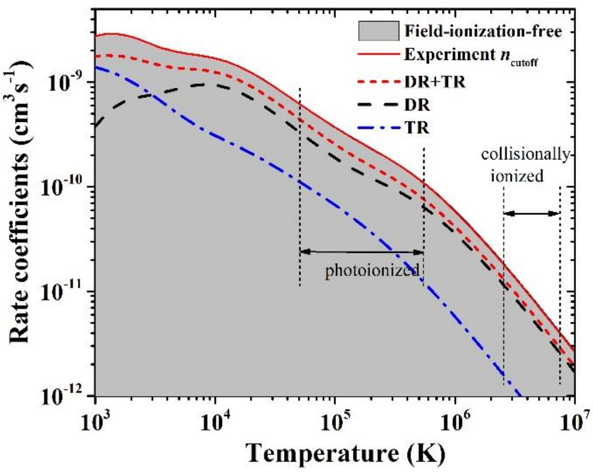

Figure 3. Plasma rate coefficents of Be-like Ar^{14+} as a function of the electron temperature. The solid red line is the experimentally-derived ΔN = 0 DR and TR rate coefficients. The theoretical results deduced from the AUTOSTRUCTURE code for ΔN = 0 DR and for TR are shown as a dotted black line and a dash-dotted blue line, respectively. The calculated sum of DR and TR is shown as a short-dashed red line. The experimentally-derived field-ionization-free plasma rate **coefficient is** shown as gray area. The approximate temperature ranges where Ar^{14+} is expected to form in photoionized plasmas and collisionally ionized plasmas are indicated by vertical dashed bars and associated arrows (Bryans, et al. 2009; Kallman & Bautista 2001).

In order to compare with other recommended theoretical data in the literature and to make convenient use of the presently measured results in plasma modeling, the Δ*N*=0 resonant plasma rate coefficients were fitted with the function

$$\alpha(T_e) = T_e^{-3/2} \sum_i c_i \times \exp(-\frac{E_i}{kT_e}) \quad (7)$$

The fit parameters of c_i and E_i are listed in Table 3, and reproduce the data within 2% at ~10^3 K and better than 1% up to 10^7 K.

Table 3. Fitted coefficients for the RR-subtracted Δ*N*=0 DR+TR rate coefficients from Figure 3 for two different values of n_{cutoff} and n_{max}=1000 (field-ionization free). The units of c_i and E_i are 10^{-3} cm^3 s^{-1} K$^{3/2}$ and eV, respectively.

No.	n_{cutoff}		n_{max}=1000	
i	c_i	E_i	c_i	E_i
1	0.254	0.12	0.244	0.115
2	0.580	0.28	0.590	0.278
3	3.74	3.47	3.77	3.45
4	5.17	1.43	5.14	1.43
5	14.3	12.42	14.38	12.45
6	23.39	31.84	23.13	31.95

7	38.84	56.39	40.30	57.03

In Figure 4, the experimentally-derived field-ionization-free plasma rate coefficients including DR and TR are compared with the theoretical data from the literature. The temperature ranges where Ar^{14+} forms in collisionally ionized plasmas and photoionized plasmas are indicated by vertical dashed bars as same as shown in Figure 3. Among the literature data, only the theoretical calculations from (Colgan, et al. 2003) and (Gu 2003) provide plasma rate coefficients at low temperatures. The calculations of (Colgan, et al. 2003) used AUTOSTRUCTURE and (Gu 2003) used FAC code. It should be noted that the plot of (Colgan, et al. 2003) as shown in Figure 4 is fitted by using the revised fit on the website of ADAS (Badnell 2009). The other calculations yielded plasma rate coefficients only at temperatures higher than 10^4 K.

At a temperature of 10^4 K, the calculated plasma rate coefficients from (Colgan, et al. 2003) and (Gu 2003) are 30% lower than experimental data. In the temperature range around 2×10^5 K, where Be-like Ar is expected to be abundant in photonionized plasmas, the calculated plasma rate coefficients from (Colgan, et al. 2003; Gu 2003; Romanik 1988) are 30% lower than the experimental results, and the data from (Mazzotta et al. 1998; Shull & Van Steenberg 1982) are about 60% lower than experimental data.

At a temperature of about 3×10^6 K where Ar^{14+} is **supposed** to be abundant in collisionally ionized plasmas, the theoretical data of (Gu 2003) are 25% lower than the experimental results. The calculated data from (Colgan, et al. 2003), (Mazzotta, et al. 1998), (Romanik 1988) and (Shull & Van Steenberg 1982) is 30%, 15%, 80%**, and** 30% higher than the experimental data. Above 6×10^6 K, the calculation of (Gu 2003) is about 25% lower than the experimental data, but the calculations of (Colgan, et al. 2003; Mazzotta, et al. 1998; Romanik 1988; Shull & Van Steenberg 1982) are all more than 30% higher than the experimental data. It should be noted that the calculation of (Gu 2003) shown in Figure 4 only included **transitions** for ΔN=0, and the data from (Colgan, et al. 2003; Mazzotta, et al. 1998; Romanik 1988; Shull & Van Steenberg 1982) shown in Figure 4 included the **transitions** for ΔN=0 and ΔN=1. As a result, DR through excitation of the 2*s* electron to higher shells ($\Delta N > 0$ DR) and also through excitation of a 1*s* electron which is not included in the experimental data could be the reason for this discrepancy. It should be noted that better than 2% between the current calculation by AUTOSTRUCTURE code (as shown in Figure 3 as a short-dashed red line) and the data from (Colgan, et al. 2003) is found if only taking into account of ΔN=0 core electron excitation. In a short summary, agreement within about 35% was found between experimentally-derived plasma rate coefficients and theoretical **calculations** by (Colgan, et al. 2003) and (Gu 2003) in the temperature range from 10^4 K to 10^7 K.

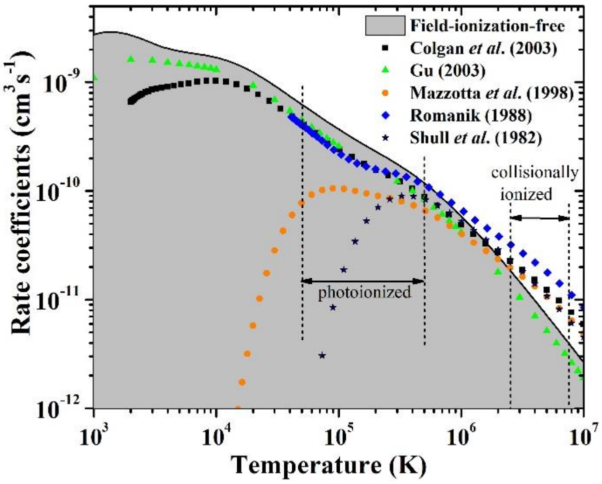

Figure *4*. Comparison of field-ionization-free resonant plasma recombination rate coefficients with theoritical calculated results of Be-like Ar. Full squares show rate coeficients by (Colgan, et al. 2003). Calculations by (Gu 2003) and (Mazzotta, et al. 1998) are shown by full triangles and full circles, respectively. Rate coefficients of (Romanik 1988) and (Shull & Van Steenberg 1982) are shown by full diamonds and stars, respectively. Temperature ranges where the Be-like Ar concentration is higher than 10% of its maximum abundance in photoionized and collisionally ionized plasmas are shown by vertical dashed bars as in Figure 3 (Bryans, et al. 2009; Kallman & Bautista 2001).

5. CONCLUSIONS

Electron-ion recombination rate coefficients of Be-like Ar^{14+} forming into B-like Ar^{13+} were derived from a measurement performed by employing the electron-ion merged-beams method at the cooler storage ring CSRm. No previous experimental results were available for this ion. The resonances associated with dielectronic ($2s^2 \rightarrow 2s2p$) and trielectronic ($2s^2 \rightarrow 2p^2$) ΔN=0 recombination within the energy range of 0−60 eV were investigated and identified by application of the Rydberg formula. Agreement in terms of DR resonance positions and strengths was found better than 10% and 30%, respectively, between the experimental recombination rate coefficient and the newly calculated results using the distorted wave code AUTOSTRUCTURE. The TR resonance positions and strenghts were also reproduced by the AUTOSTRUCTURE calculation.

For use in plasma modelling, the plasma recombination rates coefficient was deduced from the merged-beams recombination rate coefficients. The temperature range of this plasma rate coefficient is from 10^3 to 10^7 K. This range comprises the temperatures where the ions are abundant both in photoionized and collisionally ionized plasmas. The experimentally-derived plasma rate coefficient was compared with the calculated data from existing literature. At the temperature range of photoionized plasmas, the experimentally-derived rate coefficient is still up to 30% larger than the more recent results of (Gu 2003), (Romanik 1988) and (Colgan, et al. 2003). For temperatures higher than 10^6 K, the experimentally derived plasma rate coefficients are lower than the calculated data from the literature except for (Gu 2003) which only showed ΔN=0 core electron excitation. Agreement of better than 30% for the whole temperature range was found between the present experimentally-derived plasma rate coefficients and the calculated results from AUTOSTRUCTURE. Our data thus provide a stringent benchmark for Ar^{14+} recombination data used in astrophysical modelling.

Acknowledgements

This work is partly supported by the National Key R&D Program of China under Grant No. 2017YFA0402300, the National Natural Science Foundation of China through No. 11320101003, No. 91336102, No. U1732133, No. 11611530684, the Strategic Priority Research Program of the Chinese Academy of Sciences, Grant No. XDB21030900 and Key Research Program of Frontier Sciences, CAS, Grant No. QYZDY-SSW-SLH006. W. Wen thanks the support by the Youth Innovation Promotion Association CAS. S. P. Preval and N. R. Badnell acknowledge the support of EPSRC grant EP/L021803/1. S. Schippers gratefully acknowledges support by the CAS President's International Fellowship Initiative (PIFI). A helpful discussion with R. Schuch is acknowledged. The authors would like to thank the crew of Accelerator Department for skillful operation of the CSR accelerator complex.

References

Ali, S., Orban, I., Mahmood, S., Loch, S. D., & Schuch, R. 2013, A&A, 557, A2

Badnell, N. R. 2009, Atomic and Molecular Diagnostic Processes in Plasmas, http://amdppphysstrathacuk/tamoc/DATA/DR/

Badnell, N. R. 2011, Computer Physics Communications, 182, 1528

Beiersdorfer, P. 2003, Annual Review of Astronomy and Astrophysics, 41, 343

Bernhardt, D., et al. 2016, Journal of Physics B: Atomic, Molecular and Optical Physics, 49, 074004

Bernhardt, D., et al. 2015, Journal of Physics B: Atomic, Molecular and Optical Physics, 48, 144008

Bernhardt, D., et al. 2011, Physical Review A, 83, 020701

Bhatia, A. K., & Landi, E. 2008, Atomic Data and Nuclear Data Tables, 94, 223

Brandau, C., & Kozhuharov, C. 2012, in Atomic Processes in Basic and Applied Physics, eds. V. Shevelko, & H. Tawara (Berlin, Heidelberg: Springer Berlin Heidelberg), 283

Brandau, C., Kozhuharov, C., Lestinsky, M., Müller, A., Schippers, S., & Stöhlker, T. 2015, Physica Scripta, 2015, 014022

Bryans, P., Landi, E., & Savin, D. W. 2009, The Astrophysical Journal, 691, 1540
Burgess, A. 1964, The Astrophysical Journal, 139, 776
Colgan, J., Pindzola, M. S., Whiteford, A. D., & Badnell, N. R. 2003, A&A, 412, 597
Dere, K., Landi, E., Young, P., & Del Zanna, G. 2001, The Astrophysical Journal Supplement Series, 134, 331
Fogle, M., et al. 2005, A&A, 442, 757
Fritzsche, S., Surzhykov, A., & Volotka, A. 2015, New Journal of Physics, 17, 103009
Gu, M. F. 2003, The Astrophysical Journal, 590, 1131
Huang, Z. K., et al. 2015, Phys Scripta, T166, 014023
Huang, Z. K., et al. 2017, Nuclear Instruments and Methods in Physics Research Section B: Beam Interactions with Materials and Atoms, 408, 135
Kallman, T., & Bautista, M. 2001, The Astrophysical Journal Supplement Series, 133, 221
Kallman, T. R., & Palmeri, P. 2007, Reviews of Modern Physics, 79, 79
Kilgus, G., Habs, D., Schwalm, D., Wolf, A., Badnell, N. R., & Müller, A. 1992, Phys Rev A, 46, 5730
Kramida, A., Ralchenko, Y., Reader, J., & Team, N. A. 2015, Available: http://physicsnistgov/asd
Landi, E., Doron, R., Feldman, U., & Doschek, G. A. 2001, Astrophy J, 556, 912
Lepson, J., Beiersdorfer, P., Behar, E., & Kahn, S. 2003, The Astrophysical Journal, 590, 604
Müller, A. 2008, in Advances In Atomic, Molecular, and Optical Physics, eds. P. R. B. Ennio Arimondo, & C. L. Chun (Academic Press), 293
Mazzotta, P., Mazzitelli, G., Colafrancesco, S., & Vittorio, N. 1998, Astron Astrophys Suppl Ser, 133, 403
Meng, L.-J., et al. 2013, Chinese Physics C, 37, 017004
Orban, I., Böhm, S., Loch, S. D., & Schuch, R. 2008, A&A, 489, 829
Orban, I., Loch, S. D., Böhm, S., & Schuch, R. 2010, The Astrophysical Journal, 721, 1603
Orlov, D. A., et al. 2009, Journal of Physics: Conference Series, 163, 012058
Paerels, F. B. S., & Kahn, S. M. 2003, Annual Review of Astronomy and Astrophysics, 41, 291
Romanik, C. J. 1988, The Astrophysical Journal, 330, 1022
Saloman, E. B. 2010, Journal of Physical and Chemical Reference Data, 39, 033101
Savin, D. W. 2007, Journal of Physics: Conference Series, 88, 012071
Savin, D. W., et al. 2006, The Astrophysical Journal, 642, 1275
Schippers, S. 2012, Journal of Physics: Conference Series, 388, 012010
Schippers, S. 2015, Nuclear Instruments and Methods in Physics Research Section B: Beam Interactions with Materials and Atoms, 350, 61
Schippers, S., et al. 2012, Physical Review A, 85, 012513
Schippers, S., Müller, A., Gwinner, G., Linkemann, J., Saghiri, A. A., & Wolf, A. 2001, The Astrophysical Journal, 555, 1027
Schippers, S., et al. 2007, Physical Review Letters, 98, 033001
Schippers, S., Schnell, M., Brandau, C., Kieslich, S., Müller, A., & Wolf, A. 2004, A&A, 421, 1185
Schnell, M., et al. 2003, Physical Review Letters, 91, 043001
Schuch, R., & Böhm, S. 2007, Journal of Physics: Conference Series, 88, 012002
Shull, J. M., & Van Steenberg, M. 1982, The Astrophysical Journal Supplement Series, 48, 95
Träbert, E., et al. 2000, The Astrophysical Journal, 541, 506
Wang, K., et al. 2015, The Astrophysical Journal Supplement Series, 218, 16
Wen, W. Q., et al. 2013, Nucl Instrum Meth B, 317, 731
Wu, J. X., et al. 2013, Nuclear Instruments and Methods in Physics Research Section B: Beam

Interactions with Materials and Atoms, 317, Part B, 623
Zhao, H. W., et al. 2017, Physical Review Accelerators and Beams, 20, 094801